Efficient Control-Oriented Coupled Electrochemical Thermal Modeling of Li-Ion Cells

Matteo Corno **Post Conference Paper** [DELETE THIS LINE FROM YOUR ACCEPTED FINAL SUBMISSION]

***Abstract*—Lithium ion batteries are complex. Their safe and effective exploitation requires advanced Battery Management systems (BMS). This paper proposes a computationally efficient, control-oriented model of a Li-ion cell. The model describes the spatial nature of both the chemical species and temperature dynamics in a computationally efficient way. The method takes advantage of the algebraic structure that arises from the distributed nature of the model. We show that by discretizing the model PDE's with a finite difference method, the coupling equations take a Semi Separable Structure for which an efficient algebra exists. This approach yields an efficient modeling tool that can be employed for BMS design. The proposed model is validated against a high order CFD model.**

I. Introduction

Li-ion batteries are chemically unstable, and require Battery Management Systems (BMS's). The BMS continuously monitors and controls the battery states, such as: temperature, current, voltage, amount of remaining energy, and battery degradation.

It is known [1], [2] that BMS based on averaged cell models do not allow for full exploitation of the cell potential. More precisely, internal lithium concentration distribution is a crucial information to effectively avoid reaching locally critical depletion levels (and therefore damaging the battery). Similar considerations apply to the cell temperature [3], if one only monitors the surface temperature [4], [5], which is the only thermal state that is directly measurable, a thermal runaway [6] may not be promptly detected. The more accurate the model on which the BMS operates, the more effectively the cell can be used.

Several models of Li-ion batteries exist. They are classified according to their complexity and accuracy (see for example [7]). The simplest models are the equivalent circuit models (ECM's) [8]–[10], or *gray-box* models. They describe the cells dynamics with minimum computational cost by means of elementary electric circuits with voltage sources, resistors and capacitors. ECM's are easy to understand for systems engineers and are highly scalable. However, ECM's are sufficiently accurate only for relatively low and constant currents; they fail to describe the cell dynamics for medium-high dynamic currents; furthermore they offer no physical insight in the electrochemical phenomena taking place inside the cell.

First-principle electrochemical models, or *white-box* models overcome these limitations. Different first-principle modeling approaches exist: from the Single Particle Model (SPM) to advanced Computational Fluid Dynamics (CFD) models [11], that describe physical phenomena with extreme accuracy, but at the price of high computational burden and a high number of electrochemical parameters to be identified.

The Pseudo 2-Dimensional (P2D) electrochemical model, originally proposed in [12], [13] and adopted in works such as [14]–[17], is widely recognized as a valuable trade-off between detailed modeling and computational cost. It assumes spherical active material particles and it considers only two dimensions: the radial dimension, r, and the cell film thickness, named x. The P2D model, relying on Partial Differential Algebraic Equations (PDAEs), requires particular care in the implementation. Several methods are available in literature to find approximated and/or reduced-order solutions [18], [18]–[20].

The original formulation of the P2D model does not account for thermal dynamics. A number of thermal models have been developed for Li-ion cells [21]. A family of approaches uses lumped thermal models [3], [22], where the temperature gradient is neglected. This approach is based on the hypothesis that the heat generation is uniform. This hypothesis breaks under high discharge rate [23]. Many models are not bidirectionally coupled, in the sense that the electrochemical process influence the heat generation, but the cell temperature does not impact the electrochemical reactions. This drawback is overcome in [24] and [25] where the classical P2D model of a cylindrical cell is coupled with a lumped thermal model, making the physiochemical properties of the cell temperature dependent. Finally, there are works where the coupled electrochemical thermal model is solved through computational fluid dynamics, as in [11], or finite element solvers as in [26]. These methods are not suited for real-time applications and do not provide a model that is mathematically manipulable for BMS design.

In this article, that extend the work presented in [27], we present a new formulation of the P2D model for a cylindrical cell. We focus on two main contributions.

- we augment the standard P2D model with thermal dynamics. The proposed coupling is bi-directional and spatially distributed. The thermal model assumes that the temperature gradient along the cylinder axial direction

Matteo Corno is with the Dipartimento di Elettronica, Informazione e Bioingegneria, Politecnico di Milano, 20133 Milano, Italy. This work was supported by MIUR SIR project RBSI14STHV

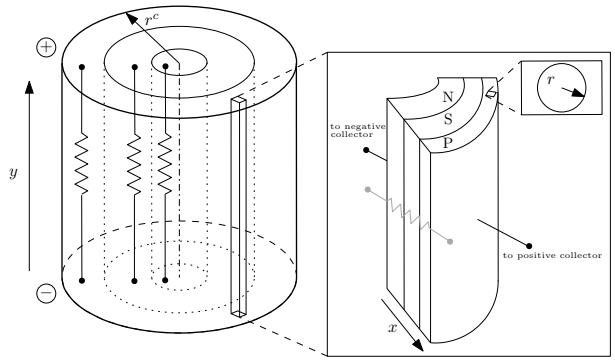

Fig. 1. Layout of a cylindrical Li-ion cell

is negligible and that the heat generation mechanisms depend on the local value of the electrochemical states.

- We propose an efficient integration scheme. We recast the nonlinear equations of the P2D model in a distributed framework. This, with minor approximations, determines the rise of specific algebraic structure, the Semi Separable Structure (SSS) [28]. The SSS defines an efficient algebra that yields a linear complexity with respect to the dimensionality. This approach also yields a closed form cell model that can be directly used for estimation and control system design as the variables retain their original physical meaning.

The paper is structured as follows. Section II recalls the continuous time partial differential equations that determine both the electrochemical and thermal dynamics. Section III presents the discretization approach and the coupling between the thermal and electrochemical parts. Section IV introduces the computationally efficient framework based on the Semi Separable Structure. Section V analyzes the model from the dynamic and computational effort stand points.

II. Lithium Ion Cell Modeling

We refer to the standard P2D model which considers only the diffusion dynamics that take place across the battery film thickness, x, and the diffusion dynamics inside the spherical particles, along the *radial direction* r (see Figure 1). The dynamics of interest can be divided into the electrochemical dynamics and the thermal dynamics.

A. Electrochemical Dynamics

The electrochemical reactions are described by three types of equations: mass balance, charge balance and kinetics equations. In our notation, t represents the time, x the spatial coordinate along the x-direction and r the spatial coordinate along the radius of the active material sphere. $c_e(t,x)$ represents the Li^+ concentration in the electrolyte, $c_s(t,r,x)$ the concentration of Li in the solid phase; $\phi_s(x,t)$ and $\phi_e(x,t)$ are respectively the potential in the solid and electrolyte phases.

Mass balances: These equations describe the conservation of Li in the solid phase (with reaction current j^{Li} from the surface)

$$\frac{\partial c_s}{\partial t} = \frac{D_s}{r^2}\overrightarrow{\nabla}_r\left(r^2\overrightarrow{\nabla}_r c_s\right) \tag{1}$$

with boundary conditions:

$$\overrightarrow{\nabla}_r c_s\Big|_{r=0} = 0; \quad D_s\overrightarrow{\nabla}_r c_s\Big|_{r=R_s} = \frac{-j^{Li}}{a_s F} \tag{2}$$

where D_s is the solid phase diffusion coefficient, F is the Faraday's constant, and a_s is the specific area of an electrode. The second mass balance is the conservation of Li in the electrolyte

$$\frac{\partial \epsilon_e c_e}{\partial t} = \overrightarrow{\nabla}_x\left(D_e^{eff}\overrightarrow{\nabla}_x c_e\right) + \frac{1-t_+^0}{F}j^{Li}. \tag{3}$$

D_e^{eff} is the effective diffusion coefficient, t_+^0 is the transference number of Li^+ with respect to the velocity of solvent (assumed to be constant). The boundary conditions are,

$$\overrightarrow{\nabla}_x c_e\Big|_{x=0} = \overrightarrow{\nabla}_x c_e\Big|_{x=L} = 0. \tag{4}$$

Charge balances: The current flowing per unit area in the solid phase, i_s, is given by Ohm's law

$$i_s(x) = -\sigma^{eff}\overrightarrow{\nabla}_x\phi_s \tag{5}$$

where σ^{eff} is the effective conductivity. At each spherical particle, the current gets diverged due to the reaction taking place between the electrode and the electrolyte. This current is in the form of flow of Li^+ and depends on the volumetric rate of electrochemical reaction j^{Li} as,

$$\overrightarrow{\nabla}_x i_s(x) = -j^{Li}; \tag{6}$$

this current adds to the electrolyte current given by,

$$\overrightarrow{\nabla}_x i_e(x) = j^{Li}. \tag{7}$$

i_e follows a modified Ohm's law which accounts for concentration variations,

$$i_e(x) = -\kappa^{eff}\overrightarrow{\nabla}_x\phi_e - \kappa_D^{eff}\overrightarrow{\nabla}_x\ln c_e\ , \tag{8}$$

here κ^{eff} is the effective ionic conductivity, κ_D^{eff} is the effective diffusion conductivity. The boundary conditions of the charge balances are: (1) the battery terminal current is the to solid phase current only

$$-\sigma_-^{eff}\overrightarrow{\nabla}_x\phi_s\Big|_{x=0} = \sigma_+^{eff}\overrightarrow{\nabla}_x\phi_s\Big|_{x=L} = \frac{I}{A} \tag{9}$$

$$\overrightarrow{\nabla}_x\phi_e\Big|_{x=0} = \overrightarrow{\nabla}_x\phi_e\Big|_{x=L} = 0 \tag{10}$$

(2) zero solid current in the separator:

$$\overrightarrow{\nabla}_x\phi_s\Big|_{x=\delta_-} = \overrightarrow{\nabla}_x\phi_s\Big|_{x=\delta_-+\delta_{sep}} = 0. \tag{11}$$

Further, there is no divergence of current within the separator and the entire terminal current flows through the separator in the form of Li^+,

$$\overrightarrow{\nabla}_x i_e(x) = 0 \tag{12}$$

$$-\kappa^{eff}\overrightarrow{\nabla}_x\phi_e - \kappa_D^{eff}\overrightarrow{\nabla}_x\ln c_e = \frac{I}{A}. \tag{13}$$

Kinetics: The above PDE's are coupled by the Butler-Volmer equation describing the reaction current at the solid/electrolyte interface:

$$j^{Li}(x) = a_s j_0 \left[\exp\left(\frac{\alpha_a F}{RT}\eta\right) - \exp\left(-\frac{\alpha_c F}{RT}\eta\right) \right] \quad (14)$$

where α_a and α_c are the anodic and cathodic transfer coefficients of electrode reaction, R the universal gas constant, T the absolute temperature in Kelvin, k is the kinetic rate constant and j_0 is the exchange current density. The overpotential η is

$$\eta = \phi_s - \phi_e - U(c_{s,e}). \quad (15)$$

The equilibrium (open circuit) voltage $U(c_{s,e})$ is evaluated as a non linear empirical function [24] of the surface stoichiometry θ.

$$\theta_-(x) = \frac{c_{s,e-}}{c_{s,max}^{anode}}; \qquad \theta_+(x) = \frac{c_{s,e+}}{c_{s,max}^{cathode}}. \quad (16)$$

For readability's sake, the above equations do not explicitly mention the temperature dependency. In reality, the exchange current density i_0, the diffusion coefficient in the solid phase D_s, the diffusion coefficient in the electrolyte phase D_e and the electrolyte ionic conductivity K all depend on the temperature according to the Arrhenius equation:

$$\Psi(T) = \Psi_{ref}\left[\frac{E_{act}^{\Psi}}{R}\left(\frac{1}{T_{ref}} - \frac{1}{T}\right)\right]$$

where Ψ is the generic parameter taken into account, Ψ_{ref} is the value of the parameter at the reference temperature $T_{ref} = 25\,^{\circ}\mathrm{C}$, R is the universal gas constant, E_{act}^{Ψ} is the activation energy of the physiochemical property.

Terminal voltage: The cell potential is given by,

$$V = \phi_s(x = L) - \phi_s(x = 0) - \frac{R_f}{A} I \quad (17)$$

where R_f is the film resistance on the electrodes surface.

B. Thermal dynamics

In deriving the thermal model, we assume that the temperature gradient along the *axial direction y* is negligible; as a consequence, we can use the 1D heat conduction in a cylinder:

$$\rho c_p \frac{\partial T}{\partial t} = k_t \frac{\partial^2 T}{\partial^2 r^c} + \frac{k_t}{r^c}\frac{\partial T}{\partial r^c} + Q \quad (18)$$

with boundary conditions:

$$\left.\frac{\partial T}{\partial r^c}\right|_{r^c=0} = 0, \qquad \left.\frac{\partial T}{\partial r^c}\right|_{r^c=R^c} = -\frac{h}{k_t}(T - T_\infty). \quad (19)$$

In the above equation, T_∞ is the environment temperature, k_t is the thermal conductivity, ρ is the density, h is the convection heat transfer coefficient, c_p is the specific heat capacity, r^c and R^c are the radial direction and the radius of the cylinder. Considering a heterogeneous cylinder, the heat capacity C_p is calculated as proposed in [29]:

$$C_p = \rho c_p = \sum_{i,k} \frac{\delta_i \varepsilon_{k,i} \rho_{k,i} c_{p,k,i}}{L} \quad (20)$$

where k indicates the phase (solid or electrolyte) and i the component (negative electrode, separator, positive electrode). Furthermore, δ_i is the thickness of the i-th component and ε_k is the volume fraction of the k-th phase in the i-th component. The volumetric heat generation rate, Q, is the sum of three terms: the volumetric reaction heat Q_j, the volumetric ohmic heat Q_o, the volumetric heat generated due to contact resistance Q_f:

$$Q_j = \frac{1}{h^c}\int_0^L j^{Li}\eta\, dx, \quad Q_f = \frac{R_f}{h^c}\tilde{i}^2,$$

$$Q_o = \frac{1}{h^c}\int_0^L \sigma^{eff}\left(\frac{\partial \phi_s}{\partial x}\right)^2 + k^{eff}\left(\frac{\partial \phi_e}{\partial x}\right)^2 + + k_D^{eff}\left(\frac{\partial ln(c_e)}{\partial x}\right)\left(\frac{\partial \phi_e}{\partial x}\right) dx.$$

In the above expressions, h^c is the height of the cylinder and $\tilde{i}$ is the specific current density. Note the dependency on electrochemical variables, which determines the coupling between the two domains (thermal and electrochemical).

III. Discretization Approach

Many techniques to solve the above partial differential equations exist. Here, we propose the use of a finite difference approach. In a cylindrical cell, the electrochemical and the thermal spatial distributions develop in two different directions. The electrochemical equations have x and r as the main geometrical direction whereas the thermal PDE develops over the cell radius r^c. As a consequence, we cannot employ a single discretization scheme. We will thus discuss the electrochemical equation discretization first, then the thermal equation and finally the coupling.

A. Electrochemical dynamics

Figure 2 graphically describes the discretization approach. The method assumes that the positive and negative electrodes consist of a series of spherical active material particles, each occupying one slice of the discretization along x with step Δx. The second discretization axis is the radial dimension r

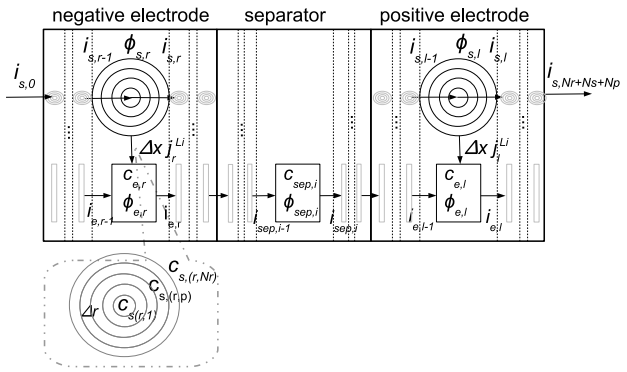

Fig. 2. Discretization of Li-ion cell along x and r dimensions

of each spherical active material particle. This discretization step is Δr. N_r, N_n, N_s and N_p are respectively the number

Species: solid phase	
$\frac{\partial c_s}{\partial t} = \frac{D_s}{r^2}\frac{\partial}{\partial r}\left(r^2\frac{\partial c_s}{\partial r}\right)$ (12)	$\dot{c}_{s,(k,p)} = \frac{D_s}{(p\Delta r)^2}\left[2p\Delta r\left(\frac{c_{s,(k,p+1)}-c_{s,(k,p)}}{\Delta r}\right) + (p\Delta r)^2\left(\frac{c_{s,(k,p-1)}-2c_{s,(k,p)}+c_{s,(k,p+1)}}{\Delta r^2}\right)\right]$ (13)
$\frac{\partial c_s}{\partial r}\Big\|_{r=0} = 0$ (14)	$c_{s,(k,1)} - c_{s,(k,0)} = 0$ (16)
$D_s\frac{\partial c_s}{\partial r}\Big\|_{r=R_s} = \frac{-j^{Li}}{a_s F}$ (15)	$D_s\left(\frac{c_{s,(k,N_r+1)}-c_{s,(k,N_r)}}{\Delta r}\right) = \frac{-j^{Li}_k}{a_s F}$ (17)
Species: electrolyte phase	
$\frac{\partial \varepsilon_e c_e}{\partial t} = \frac{\partial}{\partial x}\left(D_e^{eff}\frac{\partial c_e}{\partial x}\right) + \frac{1-t_+^0}{F}j^{Li}$ (18)	$\dot{c}_{e,k} = \frac{D_e^{eff}}{\varepsilon_e}\left(\frac{c_{e,k-1}-2c_{e,k}+c_{e,k+1}}{\Delta x^2}\right) + \frac{1-t_+^0}{F\varepsilon_e}j^{Li}_k$ (19)
$\frac{\partial c_e}{\partial x}\Big\|_{x=0} = 0$ (20)	$c_{e,1} - c_{e,0} = 0$ (22)
$\frac{\partial c_e}{\partial x}\Big\|_{x=L} = 0$ (21)	$c_{e,N_n+N_t+N_p+1} - c_{e,N_n+N_t+N_p} = 0$ (23)
Charge: solid phase	
$i_s = -\sigma^{eff}\frac{\partial \phi_s}{\partial x}$ (24)	$i_{s,k} = -\sigma^{eff}\left(\frac{\phi_{s,k+1}-\phi_{s,k}}{\Delta x}\right)$ (25)
$\frac{\partial \phi_s}{\partial x}\Big\|_{x=\delta_n} = \frac{\partial \phi_s}{\partial x}\Big\|_{x=\delta_n+\delta_s} = 0$ (26)	$i_{s,N_n} = i_{s,N_n+N_t} = 0$ (28)
$-\sigma^{eff}\frac{\partial \phi_s}{\partial x}\Big\|_{x=0} = -\sigma^{eff}\frac{\partial \phi_s}{\partial x}\Big\|_{x=L} = \frac{I}{A}$ (27)	$i_{s,0} = i_{s,N_n+N_t+N_p} = \frac{I}{A}$ (29)
Charge: Electrolyte Phase	
$i_e = -k^{eff}\frac{\partial \phi_e}{\partial x} - k_D^{eff}\frac{\partial}{\partial x}ln(c_e)$ (30)	$i_{e,k} = -k^{eff}\left(\frac{\phi_{e,k+1}-\phi_{e,k}}{\Delta x}\right) - k_D^{eff}\left(\frac{ln(c_{e,k+1})-ln(c_{e,k})}{\Delta x}\right)$ (31)
$\frac{\partial \phi_e}{\partial x}\Big\|_{x=0} = 0$ (32)	$\phi_{e,1} - \phi_{e,0} = 0$ (34)
$\frac{\partial \phi_e}{\partial x}\Big\|_{x=L} = 0$ (33)	$\phi_{e,N_n+N_t+N_p+1} - \phi_{e,N_n+N_t+N_p} = 0$ (35)

Fig. 3. Electrochemical model equations and their discretization.

of finite elements of the sphere, of the negative electrode, of the separator and of the positive electrode discretization. Each discretized region has a lumped electrolyte phase Li^+ concentration c_e and electrolyte phase potential ϕ_e (named c_{sep} and ϕ_{sep} in the separator). Each sphere has a lumped solid phase potential ϕ_s and a volumetric rate of electrochemical reaction, j^{Li}, while the solid phase Li concentration is distributed along r. The currents, i_s and i_e, exhibit a gradient along x.

The discretization of the equations that govern the electrochemical processes is summarized in Figure 3

The model has $(N_r+1)N_p + (N_r+1)N_n + N_s$ dynamic equations, coupled by j_k^{Li} through a non-linear algebraic system.

B. Thermal dynamics

The thermal dynamics are discretized with a finite difference method along the radial direction. The cell is is divided in a number (N_c) of concentrical cylindrical cells with Δr^c step, determined according to a constant volume approach. The discretization of (18) results in:

$$\rho c_p \dot{T}_z = k_t\left[\frac{T_{z-1}-2T_z+T_{z+1}}{(\Delta r_z^c)^2}\right] + \frac{k_t}{r_z^c}\left[\frac{T_{z+1}-T_z}{\Delta r_z^c}\right] + Q_z$$

where T_z, r_z, and Q_z are respectively the temperature, the radius and the heat generation rate of the z-th element. The term Δr_z is defined as:

$$\Delta r_z^c = r_z^c - r_{z-1}^c$$

where:

$$r_0^c = 0, \qquad r_{N_c}^c = R^c$$

with boundary conditions

$$T_1 - T_0 = 0, \qquad \frac{T_{N_c+1}-T_{N_c}}{\Delta r_{N_c}^c} = -\frac{h}{k_t}(T_{N_c} - T_\infty).$$

C. Coupling

The two discretization approaches need to be mapped one onto the others. Cylindrical cells are obtained by winding up a thin sandwiched sheet in a cylinder (Figure 1). The Li-ion cell is thus viewed as N_c subcells in parallel where each subcell is described by an electrochemical set of equations and characterized by its own temperature. The thermal model describes the heat diffusion through the different subcells. The coupling is determined by the Arrhenius equation. The discretized heat generation rate Q_z of the z-th subcell is:

$$\begin{aligned}
Q_z &= Q_{j,z} + Q_{o,z} + Q_{f,z} \\
Q_{j,z} &= \frac{1}{h^c}\sum_i j_{i,z}^{Li}\eta_{i,z}\Delta x \\
Q_{o,z} &= \frac{1}{h^c}\sum_i\left[\sigma^{eff}\left(\frac{\phi_{s,i+1,z}-\phi_{s,i,z}}{\Delta x}\right)^2\Delta x\right] + \\
&+ \frac{1}{h^c}\sum_i\left[k^{eff}\left(\frac{\phi_{e,i+1,z}-\phi_{e,i,z}}{\Delta x}\right)^2\Delta x\right] + \\
&+ \frac{1}{h^c}\sum_i\left[k_D^{eff}\left(\frac{ln(c_{e,i+1,z})-\ln(c_{e,i,z})}{\Delta x}\right)\right. \\
&\left.\left(\frac{\phi_{e,i+1,z}-\phi_{e,i,z}}{\Delta x}\right)\Delta x\right] \\
Q_{f,z} &= \frac{R_f}{h^c A_z^2}\left(\widehat{I}_z\right)^2
\end{aligned}$$

The term $\widehat{I}_z$ represents the input current of the z-th subcell. The parallel connection of the subcells impose that:

$$I = \sum_{z=1\ldots N_c}\widehat{I}_z \tag{21}$$

The model has $N_c\left[(N_r+1)(N_n+N_p)+N_s\right]$ ODE's, that are coupled by the Butler-Volmer equation in groups of $\left[(N_r+1)(N_n+N_p)+N_s\right]$ and a set of N_c-1 constraint-type-equations:

$$V_{z+1} - V_z = 0 \quad \text{with} \quad z \in [1, N_c-1]\,. \tag{22}$$

The coupling of the impedance-like causality of the P2D model with these constraints is not trivial. The following section introduces a numerical efficient integration scheme to treat the system.

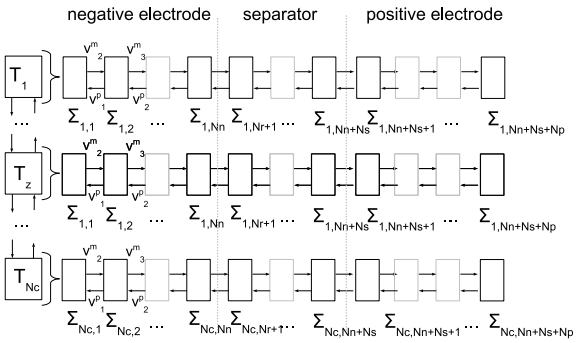

Fig. 4. Li-ion cell as spatially distributed string interconnected system.

IV. Integration Scheme

The proposed integration scheme stems from considering the discretized system as a Spatially Interconnected System. The cells represent a series of dynamical systems that communicate through interface variables. Figure 4 depicts this. The communication happens on different scales: each element of the electrochemical discretization communicates with the adjacent ones and each string of cell is influenced by the other strings through the thermal dynamics.

A. Spatially Interconnected Systems

To better understand the approach, let us consider a single string of Figure 4. A string of N_{tot} dynamical subsystems of the form:

$$\begin{aligned} \dot{x}_k &= f_k\left(x_k, v_k^p, v_k^m, u_k\right) \\ v_{k-1}^p &= g_k^p\left(x_k, u_k, v_k^p, v_k^m\right) \\ v_{k+1}^m &= g_k^m\left(x_k, u_k, v_k^p, v_k^m\right) \\ y_k &= h_k\left(x_k, v_k^p, v_k^m, u_k\right) \end{aligned} \tag{23}$$

takes the name of Spatially Distributed String Interconnected System [28]. Such systems can be either strictly spatially proper or not depending on whether g_k^p and g_k^m are dependent on v_k^m and v_k^p, respectively. Let us start considering a strictly spatially proper system. In this case, the interconnecting variables can be easily eliminated through a process called *lifting*; this yields a $N_{tot}N_{sub}$ order system (N_{sub} being the order of the subsystem). The computational complexity of integrating the complete system with standard ODE solvers grows as $\mathrm{O}\big((N_{tot}N_{sub})^3\big)$.

On the other hand, preserving the distributed nature of the system and simulating each subsystem independently yields an improvement of computational efficiency. Preserving the distributed nature requires sampling the interconnecting variables at frequency h. The integration routine simulates the N_{tot} subsystems independently at a shorter integration step and computes the interface variables at a lower sampling rate. This approximation yields a computational complexity to $\mathrm{O}\big(N_{tot}N_{sub}^3\big)$ or even $\mathrm{O}\big(N_{sub}^3\big)$ - if a parallel architecture with N_{tot} cores is available. Note that the under sampling of the interconnecting variables may introduce errors. The entity of the errors depend on how much the internal dynamics is coupled to the dynamics of the interconnecting variables.

In the case of non spatially strictly proper systems the situation is more complex. If g_k^p or g_k^m are dependent on v_k^m and v_k^p, it is, in general, not possible to write the subsystems in explicit form. The case of linear dependency represents a special case for which we propose an efficient method. Assume that

$$\begin{aligned} \dot{x}_k &= f_k\left(x_k, v_k^p, v_k^m, u_k\right) \\ v_{k-1}^p &= g_{k1}\left(x_k, u_k\right) + W_k^p v_k^p + Z_k^m v_k^m \\ v_{k+1}^m &= g_{k2}\left(x_k, u_k\right) + Z_k^p v_k^p + W_k^m v_k^m \\ y_k &= h_k\left(x_k, v_k^p, v_k^m, u_k\right) \end{aligned} \tag{24}$$

then the interconnecting equations can be arranged in a linear system of the form $Ev = b(x, u)$ where,

$$v = \begin{bmatrix} v_1^p \\ v_2^m \\ v_2^p \\ \vdots \\ v_{N-1}^m \\ v_{N-1}^p \\ v_N^m \end{bmatrix} \quad b = \begin{bmatrix} g_{12}\left(x_1, u_1\right) \\ g_{21}\left(x_2, u_2\right) \\ g_{22}\left(x_2, u_2\right) \\ \vdots \\ g_{(N-1)1}\left(x_{(N-1)}, u_{(N-1)}\right) \\ g_{(N-1)2}\left(x_{(N-1)}, u_{(N-1)}\right) \\ g_{N1}\left(x_N, u_N\right) \end{bmatrix}. \tag{25}$$

The spatially distributed nature of the system makes E a Sequentially Semi Separable matrix [28] encoded as:

$$E = SSS\left(L_s, M_s, N_s, O_s, P_s, Q_s, R_s\right) \tag{26}$$

where,

$$\begin{aligned} &L_s = \begin{bmatrix} I \\ 0 \end{bmatrix} \ \forall s \in \{2, 3, \cdots, N-1\}, \ L_N = I \\ &M_s = 0 \ \forall s \in \{2, 3, \cdots, N-1\} \\ &N_1 = I, \ N_s = \begin{bmatrix} 0 & I \end{bmatrix} \ \forall s \in \{2, 3, \cdots, N-1\} \\ &O_1 = -Z_1^p, \ O_N = -Z_N^m \\ &O_s = \begin{bmatrix} -Z_s^m & -W_s^p \\ -W_s^m & -Z_s^p \end{bmatrix} \ \forall s \in \{2, 3, \cdots, N-1\}, \\ &P_1 = I, \ P_s = \begin{bmatrix} 0 \\ I \end{bmatrix} \ \forall s \in \{2, 3, \cdots, N-1\} \\ &Q_s = 0 \ \forall s \in \{2, 3, \cdots, N-1\} \\ &R_s = \begin{bmatrix} I & 0 \end{bmatrix} \ \forall s \in \{2, 3, \cdots, N-1\}, \ R_N = I \end{aligned} \tag{27}$$

Semi Separable matrices define an algebra for which efficient algorithms exist. In particular, the system of equations $Ev = b(x, u)$ is solvable in $\mathrm{O}(N_{tot})$. If E is invertible the system is well posed [30] and the interconnecting variables can be computed in a centralized block before the integration of each subsystem.

The same approach can still be applied if the other strings are added to the picture. The constraints imposed by the connection between strings can be added to E. The augmentation of E may change its structure; we will show in what follows that the constraints that arise from the parallel connection can still be managed efficiently.

In the remainder of the section, we will first show that the single subcell can be cast into a string of interconnected systems and subsequently we will address the inter-string constraints.

B. Spatially Interconnected Li-ion Subcell Model

Let us consider the generic subcell of Figure 4. Figure 5 shows the k^{th} finite element with its interfacing variables. The state equations for the subsystems are the N_r dynamic equations for the solid and one for the electrolyte diffusion.

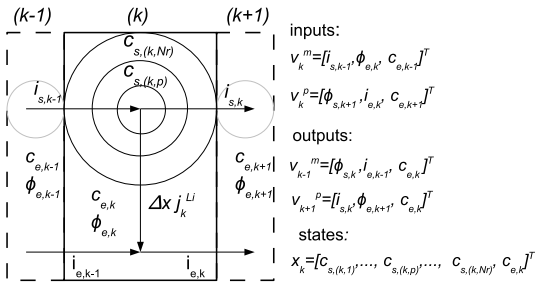

Fig. 5. A single discretized part of positive / negative electrode interconnected with neighboring blocks shown as dotted

They depend on j_k^{Li}. By eliminating ϕ_{sk} from equation (14) using equation (5) and then eliminating i_{sk} using the discretized version of equation (6) we get j_k^{Li} as an implicit function of states, inputs but also j_k^{Li} itself. Its linearization brings yields the explicit form (as also done in [24]):

$$j_k^{Li} = \frac{a_s}{R_{ct}} \left[\phi_{sk} - \phi_{ek} - U\left(c_{s(k,N_r)}\right) \right] \tag{28}$$

where,

$$R_{ct} = \frac{RT}{j_0 F\left(\alpha_a + \alpha_c\right)}$$

Substituting the linearized j_k^{Li} in the dynamic equations, we obtain the following state equations,

$$\dot{x}_k = \begin{bmatrix} -\alpha_1 & \alpha_1 & 0 & ... & 0 \\ \frac{D_s}{\Delta r^2} & -\alpha_2 & \alpha_2 & ... & 0 \\ ... & ... & ... & ... & ... \\ 0 & ... & \frac{D_s}{\Delta r^2} & -\frac{D_s}{\Delta r^2} & 0 \\ 0 & ... & 0 & 0 & -\frac{2D_e^{eff}}{\epsilon_e \Delta x^2} \end{bmatrix} x_k + \begin{bmatrix} 0 \\ 0 \\ ... \\ -\Omega\ U\left(x_k\left(N_r\right)\right) \\ -\gamma\ U\left(x_k\left(N_r\right)\right) \end{bmatrix} + \begin{bmatrix} 0 & 0 & 0 \\ 0 & 0 & 0 \\ ... & & ... \\ \Omega & 0 & 0 \\ \gamma & 0 & \frac{D_e^{eff}}{\epsilon_e \Delta x^2} \end{bmatrix} v_k^p + \begin{bmatrix} 0 & 0 & 0 \\ 0 & 0 & 0 \\ ... & & ... \\ \Omega \frac{\Delta x}{\sigma^{eff}} & -\Omega & 0 \\ \gamma \frac{\Delta x}{\sigma^{eff}} & -\gamma & \frac{D_e^{eff}}{\epsilon_e \Delta x^2} \end{bmatrix} v_k^m \tag{29}$$

where

$$\begin{array}{cc} \Omega = -\frac{1}{\beta R_{ct}} \left(\frac{2}{N_r \Delta r F} + \frac{1}{\Delta r F} \right) & \gamma = \frac{a_s}{\beta R_{ct}} \left(\frac{1-t_+^0}{F} \right) \\ \beta = 1 + \frac{\Delta x^2}{\sigma^{eff}} \frac{a_s}{R_{ct}} & \alpha_i = \left(\frac{2D_s}{i \Delta r} + \frac{D_s}{\Delta r^2} \right) \end{array} \tag{30}$$

and, defining some constants

$$\begin{array}{cccc} M_1 = \frac{\Delta x a_s}{\beta R_{ct}} & M_2 = \frac{\Delta x^2}{\sigma^{eff}} \frac{a_s}{\beta R_{ct}} & & \\ M_3 = \frac{\Delta x}{\sigma^{eff}} & M_4 = -\frac{\Delta x}{\kappa^{eff}} & K_d K = \frac{\kappa_D^{eff}}{\kappa^{eff}}, & \end{array} \tag{31}$$

the output relation equations can be derived as

$$v_{k-1}^p = \begin{bmatrix} M_2 U\left(x_k\left(N_r\right)\right) \\ M_1 U\left(x_k\left(N_r\right)\right) \\ x_k\left(N_r+1\right) \end{bmatrix} + \begin{bmatrix} (1-M_2) & 0 & 0 \\ -M_1 & 1 & 0 \\ 0 & 0 & 0 \end{bmatrix} v_k^p + \begin{bmatrix} M_3(1-M_2) & M_2 & 0 \\ -M_2 & M_1 & 0 \\ 0 & 0 & 0 \end{bmatrix} v_k^m \tag{32}$$

$$v_{k+1}^m = \begin{bmatrix} M_1 U\left(x_k\left(N_r\right)\right) \\ K_d K \ln\left(x_k\left(N_r+1\right)\right) \\ x_k\left(N_r+1\right) \end{bmatrix} + \begin{bmatrix} -M_1 & 0 & 0 \\ 0 & M_4 & 0 \\ 0 & 0 & 0 \end{bmatrix} v_k^p + \begin{bmatrix} -(M_2-1) & M_1 & 0 \\ 0 & 1 & 0 \\ 0 & 0 & 0 \end{bmatrix} v_k^m + \begin{bmatrix} 0 \\ -K_d K \ln\left(v_k^p\left(N_r\right)\right) \\ 0 \end{bmatrix} \tag{33}$$

The separator and the interfaces between the terminals and the electrodes and the electrodes are amenable to the same procedure. This results in a system in the form of (23). From the analysis of the above system two conclusions are due: (1) the interconnecting output variables are only weakly coupled to the Li diffusion in the active material; in fact only the last element $x_k(N_r)$ appears in the above equations. (2) Although the subsystems are not directly in the *linear in interconnecting variables* form, the only nonlinear term in the equation depends on $v_k^p\left(N_r\right)$ which is a state of the neighboring block and is thus available for solving the system $Ev = b$.

Following the above procedure, one gets to N_c independent set of equations; each string has as inputs the current flowing in that subcell ($\widehat{I}_z$) and the temperature, while its output is the terminal voltage. At this stage the subcell current is still undermined. Recall now that the N_c cells are connected in parallel, this imposes the constraints (21) and (22). Including these constraints in the above formulation, one gets:

$$\begin{bmatrix} E_{tot} & \mathbf{0}_{N_c \times N_c} \\ C_{v,tot} & C_{I,tot} \\ \mathbf{0}_{1 \times N_c} & \mathbf{1}_{1 \times N_c} \end{bmatrix} \begin{bmatrix} v_{tot} \\ I_{tot} \end{bmatrix} = \begin{bmatrix} b_{tot} \\ \mathbf{0}_{N_c \times 1} \\ I \end{bmatrix} \tag{34}$$

where the unknown v_{tot} and I_{tot} are respectively the stacked vector of the v for each subcell and stacked vector of the subcell currents. Similarly, b_{tot} is the stacked vector of all b. E_{tot} is the block-diagonal matrix of E defined above; $[C_{v,tot}\, C_{I,tot}]$ is the $(N_c - 1) \times 2N_c$ matrix that selects the potential of the first element of the negative and the last element of the positive electrode and the current for pairs of subcell according to (17) to impose the constraint (22). The bottom row of (34) translates (21) in matrix form.

Inspection of (34) reveals that the addition of the parallel constraints breaks the SSS structure; however one notice that the equations are in the form of a block triangular system of equations. This means that at each sampling time, the

SSS systems of equation of the form $Ev = b$ can be solved independently as in the case of the single subcell and subsequently the subcell currents can be computed solving the bottom half of the system.

We thus define the integration routine summarized in Figure 6. At each integration step, the state dependent parameters are

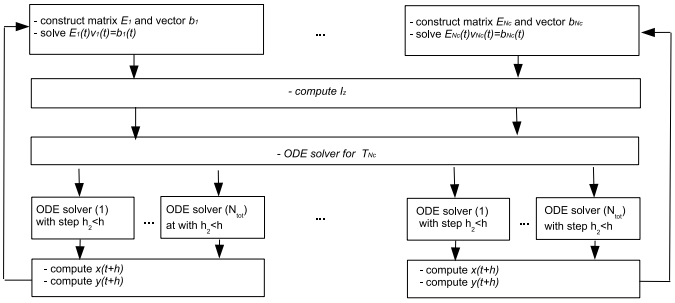

Fig. 6. Li-ion cell simulator - algorithm

updated according to the previously computed value of the states; these values are entered in the E_z matrices and the b_z vectors. The SSS algebra is used to solve for the interconnected variables v at a sampling step h. The interconnecting variables v along with the other variables are used to compute the current through each subcell. The current through each subcell along with the electrochemical variable available in v drives the discretized thermal dynamics. After that, all the subsystems of each subcell can be simulated using an ODE solver of choice keeping the interconnecting variables and subcell temperature constant.

V. Model Analysis and Results

This section analyzes the simulation results of the proposed model. We focus on mainly three aspects: tuning of the discretization, comparison with a complete CFD model and computational efficiency analysis. The reference cell model is the one in [22], [24].

A. Model Tuning

It is useful to discuss the choice of the value of some discretization variables. In the sake of clarity and conciseness, we focus on two parameters: the choice of N_r and that of N_c.

Figure 7 shows the terminal voltage and solid phase surface concentration $c_{s,e}$ for different levels of discretization N_r. In the simulation, a current of 10 C is drawn for 20s from an initial state of charge of 100%. In the simulation $N_n = N_p = 5$, $N_s = 3$ and $h = 0.05s$. The second subplot of 7 shows the surface concentration at time 2 s. The dimension x is normalized with respect to the total length of the cell L. The figure shows that increasing N_r has an impact on the terminal voltage response; however, using N_r greater than 50 does not seem to have any benefit.

Subsequently, we analyze the choice of the thermal model discretization. In order, to more realistically excite the thermal dynamics, we simulate the cell under conditions similar to the ones encountered by a cell in a Hybrid Electric Vehicle battery

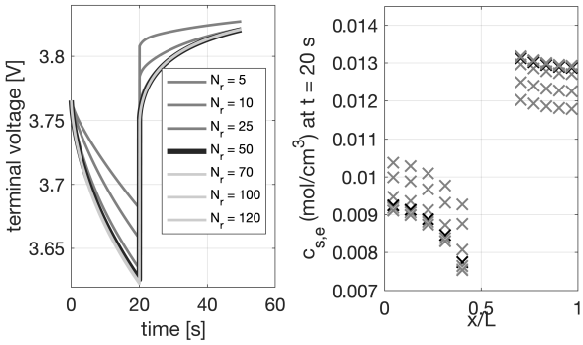

Fig. 7. Effect of different levels of discretization of the spherical active material particle.

pack. We simulate 4 repetitions of the US06 driving cycle, scaling the battery pack so that the cell reaches maximum current of 25 C, and a mean current of 1 C. The initial temperature is $T_\infty = 25\,^\circ\mathrm{C}$. The heat transfer coefficient h is set to the value of $60\frac{W}{m^2K}$. Figure 8 plots two indexes that summarizes the thermal behavior:

- The index ΔT quantifies the difference between the core and the surface:

$$\Delta T = T_1 - T_{N_c}.$$

- The index δT measures the difference between the cell average temperature and the environment:

$$\delta T = T_{bulk} - T_\infty$$

where the average temperature is:

$$T_{bulk} = \frac{\sum_{z=1}^{N_c} V_z^s \cdot T_z}{\sum_{z=1}^{N_c} V_z^s}$$

with V_z^s represents the volume of the z-th subcell.

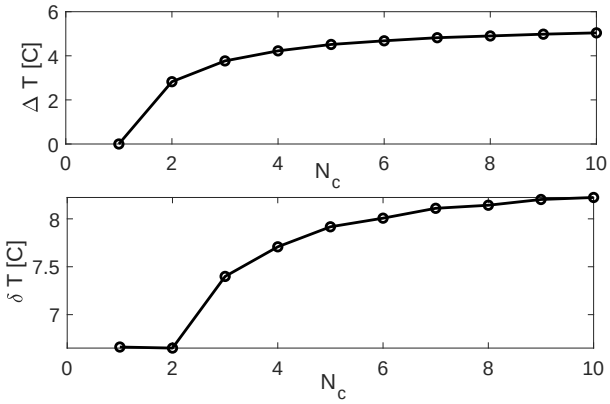

Fig. 8. Sensitivity analysis with respect to N_c

The indexes show that the temperature gradient is not negligible. However, $N_c = 6$ is enough to accurately describe the temperature dynamics. From now on, we will refer to $N_c = 6$.

B. Model Comparison

The proposed integration scheme requires some assumptions and simplifications. In order to assess the effects of these simplifications, we compare the outputs of our model against an experimentally validated CFD model [15]. The choice of using a CFD model allows for a more accurate comparison of the internal variables which are not easily measurable. The model validation details three main aspects terminal voltage, concentration gradients along x, and response to transient currents.

Figure 9 plots the results of a constant current discharge experiment performed from a fully charged battery with three current levels. We consider two types of simulations, the first one (solid line) neglects the temperature dynamics (considering all subcells at the same temperature). The second type of simulation considers the entire model as described. The plot shows the terminal voltage and the temperature

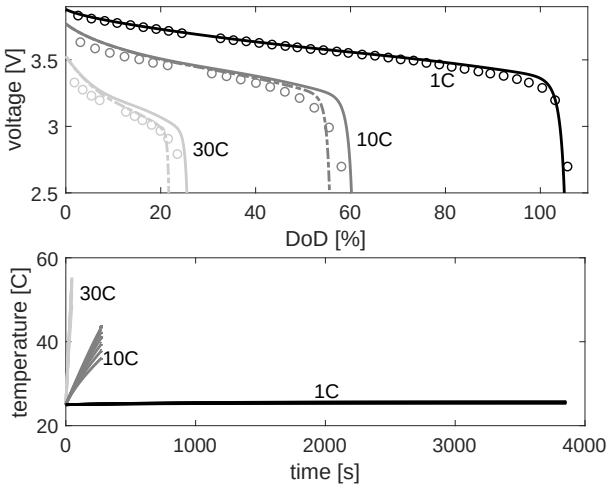

Fig. 9. Terminal voltage prediction of model at different C-rates: (-) Discretized model, (o) CFD mode.

dynamics for each of the N_c subcells. The terminal voltage is plotted with respect to the Depth of Discharge (DoD), whereas the temperature is time-based. From figure, a numbers of conclusions are due:

- The model is accurate in the entire DoD range for 1C; for higher currents the accuracy range is reduced toward the end of discharge. The error at higher currents is due to the nonlinearity in the terminal voltage characteristic $U\left(c_{s,e}\right)$. Because of that small errors in $c_{s,e}$ result in large errors in voltage.
- In the case of 1 C, the temperature dynamics do not play an important role. 1 C is not enough to heat the battery. As the C rate increases we see that the temperature dynamics considerably affects the discharge dynamics.
- For the higher C rates, a temperature gradient builds in the cell. At the end of the discharge the temperature difference between the core and the surface of the cell gets to 20 degrees.

One of the advantages of using an electrochemical model resides in the possibility of accurately modeling the evolution of the species gradients. Figure 10 compares the proposed model and the CFD model. The figure provides a snapshot at 20 seconds during a constant current (5C) discharge of the electrochemical reaction at the solid/ electrolyte interface j^{Li}, the surface concentration and the Li concentration in the electrolyte as a function of the position. The model correctly

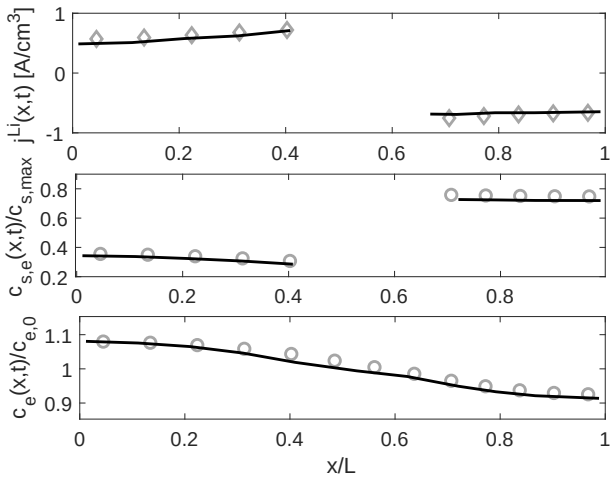

Fig. 10. Gradients along the x dimension. The continuous line is the CFD model, whereas the circles represent the model.

describes the gradients along the x direction.

The final comparison with the CFD model is carried out in terms of dynamic response. Figure 11 plots the terminal voltage and the temperature evolution for a test consisting of a series of current steps. Also in this case, the model correctly

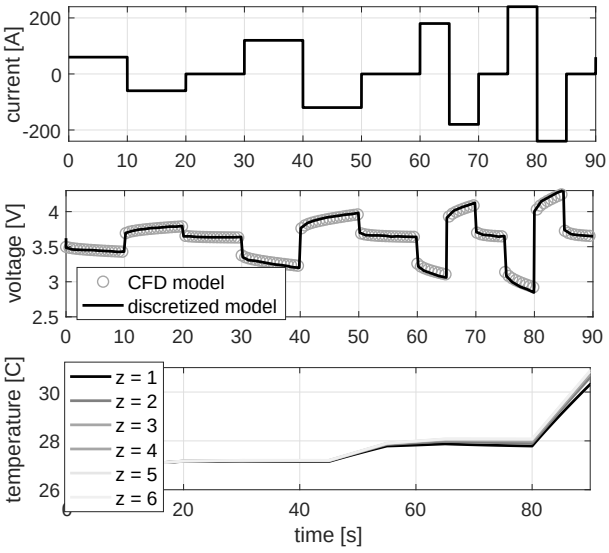

Fig. 11. Results of the transient current simulation: current, voltage and temperature.

captures the voltage dynamics. Note that despite the extremely high currents, this short test does not develop an appreciable temperature gradient.

Figure 12 illustrates the advantages of a coupled bi-directional and spatially distributed thermal model. It plots the comparison of the surface concentration dynamics in the first element of the negative electrode (top subplot) and in the last element of the positive electrode (bottom subplot)

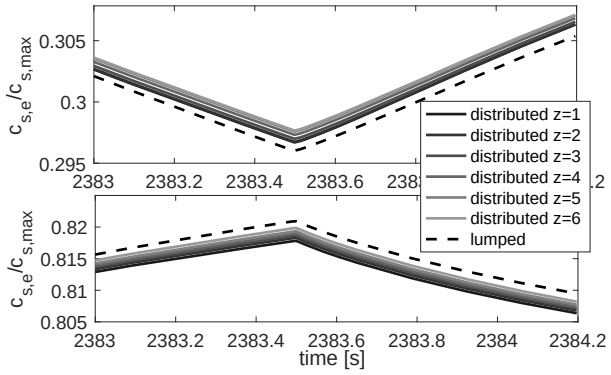

Fig. 12. Comparison of the concentrations dynamics.

for the lumped thermal model ($N_c = 1$ - dashed line) and for the distributed model ($N_c = 6$ - solid line); the darkest solid line refers to the inner subcell, while the lighter solid line refers to the outer subcell. The figure plots a snapshot of the state of the cell during the US06 cycle. The temperature considerably affects the intercalation dynamics, therefore, if the internal temperature gradient is not negligible, the lithium concentration is not uniform along the radial direction r^c.

C. Complexity Analysis

The use of the spatially interconnected framework enables two computational advantages: 1) the coupling equations can be solved in linear complexity with respect to the discretization along x, and 2) the integration is amenable to a high degree of parallelization. In fact, recalling Figure 6, the integration of each cell can be run in parallel. Figure 13 shows the simulation time with different discretization levels of positive electrode, negative electrode and separator keeping the discretization of spherical active material particle constant and the computation time for varying radial discretizations. The figure plots the

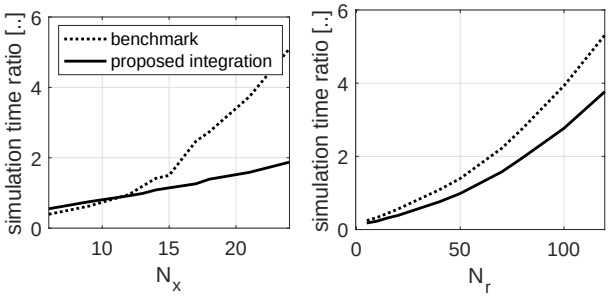

Fig. 13. Simulation time per step for different discretization levels

simulation time ratio (the ratio between the time it takes to simulate a given amount of time and that time) for an implementation of the model that does not exploit the spatially interconnected framework and the proposed approach. The figure deserves a few comments:

- increasing the discretization along x causes a linear increase in the simulation time. Whereas, in the benchmark approach, the increase in computation time is more than linear.
- For low level of discretization, the proposed method comes with an overhead that makes the benchmark approach more efficient.
- When the radial discretization increases, the simulation time does not grow linearly as the method does not exploit any structure in the r dimension.

The above analysis indicates that a discretization of $N_r = 50$, $N_n = 5$, $N_p = 5$ and $N_s = 3$, $N_c = 6$ guarantees real time simulation on the adopted platform[1].

VI. Conclusions

This work presents a control-oriented electrochemical model of a Li-ion cell that accounts for the thermal dynamics in a coupled way: the electrochemical reaction determines the thermal dynamics and vice versa. After having described the equation, we spatially discretize the equation using a finite difference method. Following this approach, the cell equations take the form of a spatially interconnected system; we show that, exploiting minor approximations, the complexity of integrating the equation can be considerably reduced. The proposed modeling approach, relying only on two approximations (linearization of the Butler-Volmer Kinetics and the holding of the interconnecting variables), has several advantages:

- It provides an efficient simulator that captures the mass diffusion dynamics of the Li-ion cell and the thermal gradients of the cell battery;
- it avoids any iterative solution of nonlinear equations, thus improving efficiency and avoiding possible non convergent behavior;
- when linearized, the state space model assumes an SSS structure that can further exploited in the design and implementation of control systems [28], [31], [32];
- it is amenable to parallelization, thus improving even further the computational efficiency.

The second part of the paper analyzes the model properties, focusing on the effect of the approximations, the choice of the discretization and the effect of the coupled dynamics. In conclusion, the approximation does not greatly affect the accuracy of the model, while providing a useful tool for Battery Management System design.

References

[1] K. A. Smith, C. D. Rahn, and C. Y. Wang. Model-based electrochemical estimation and constraint management for pulse operation of lithium ion batteries. *IEEE Transactions on Control Systems Technology*, 18(3):654–663, May 2010.

[2] Kandler Smith and Chao-Yang Wang. Power and thermal characterization of a lithium-ion battery pack for hybrid-electric vehicles. *Journal of power sources*, 160(1):662–673, 2006.

[3] Christophe Forgez, Dinh Vinh Do, Guy Friedrich, Mathieu Morcrette, and Charles Delacourt. Thermal modeling of a cylindrical lifepo 4/graphite lithium-ion battery. *Journal of Power Sources*, 195(9):2961–2968, 2010.

[4] Robert R Richardson and David A Howey. Sensorless battery internal temperature estimation using a kalman filter with impedance measurement. *IEEE Transactions on Sustainable Energy*, 6(4):1190–1199, 2015.

[5] Languang Lu, Xuebing Han, Jianqiu Li, Jianfeng Hua, and Minggao Ouyang. A review on the key issues for lithium-ion battery management in electric vehicles. *Journal of power sources*, 226:272–288, 2013.

[1] MacBook Pro 2.8 GHz Intel Core i7 16 Giga RAM

[6] Qingsong Wang, Ping Ping, Xuejuan Zhao, Guanquan Chu, Jinhua Sun, and Chunhua Chen. Thermal runaway caused fire and explosion of lithium ion battery. *Journal of Power Sources*, 208:210 – 224, 2012.

[7] Paul WC Northrop, Bharatkumar Suthar, Venkatasailanathan Ramadesigan, Shriram Santhanagopalan, Richard D Braatz, and Venkat R Subramanian. Efficient simulation and reformulation of lithium-ion battery models for enabling electric transportation. *Journal of The Electrochemical Society*, 161(8):E3149–E3157, 2014.

[8] Lijun Gao, Shengyi Liu, and R. A. Dougal. Dynamic lithium-ion battery model for system simulation. *IEEE Transactions on Components and Packaging Technologies*, 25(3):495–505, Sep 2002.

[9] R. C. Kroeze and P. T. Krein. Electrical battery model for use in dynamic electric vehicle simulations. In *IEEE Power Electronics Specialists Conference*, pages 1336–1342, June 2008.

[10] K. Li, F. Wei, K. J. Tseng, and B. Soong. A practical lithium-ion battery model for state of energy and voltage responses prediction incorporating temperature and ageing effects. *IEEE Transactions on Industrial Electronics*, 65(8):6696–6708, Aug 2018.

[11] CY Wang and Venkat Srinivasan. Computational battery dynamics (cbd) - electrochemical/thermal coupled modeling and multi-scale modeling. *Journal of power sources*, 110(2):364–376, 2002.

[12] Marc Doyle, Thomas F Fuller, and John Newman. Modeling of galvanostatic charge and discharge of the lithium/polymer/insertion cell. *Journal of the Electrochemical Society*, 140(6):1526–1533, 1993.

[13] Thomas F Fuller, Marc Doyle, and John Newman. Simulation and optimization of the dual lithium ion insertion cell. *Journal of the Electrochemical Society*, 141(1):1–10, 1994.

[14] Kandler Smith and Chao-Yang Wang. Solid-state diffusion limitations on pulse operation of a lithium ion cell for hybrid electric vehicles. *Journal of Power Sources*, 161(1):628–639, 2006.

[15] Kandler A Smith, Christopher D Rahn, and Chao-Yang Wang. Control oriented 1d electrochemical model of lithium ion battery. *Energy Conversion and management*, 48(9):2565–2578, 2007.

[16] Nalin A Chaturvedi, Reinhardt Klein, Jake Christensen, Jasim Ahmed, and Aleksandar Kojic. Algorithms for advanced battery-management systems. *IEEE Control Systems*, 30(3):49–68, 2010.

[17] Adrien M. Bizeray, Shi Zhao, Stephen Duncan, and David A. Howey. Lithium-ion battery thermal-electrochemical model-based state estimation using orthogonal collocation and a modified extended kalman filter. *CoRR*, abs/1506.08689, 2015.

[18] Ali Jokar, Barzin Rajabloo, Martin Désilets, and Marcel Lacroix. Review of simplified pseudo-two-dimensional models of lithium-ion batteries. *Journal of Power Sources*, 327:44–55, 2016.

[19] Yi Zeng, Paul Albertus, Reinhardt Klein, Nalin Chaturvedi, Aleksandar Kojic, Martin Z Bazant, and Jake Christensen. Efficient conservative numerical schemes for 1d nonlinear spherical diffusion equations with applications in battery modeling. *Journal of The Electrochemical Society*, 160(9):A1565–A1571, 2013.

[20] Dong Zhang, Branko N Popov, and Ralph E White. Modeling lithium intercalation of a single spinel particle under potentiodynamic control. *Journal of The Electrochemical Society*, 147(3):831–838, 2000.

[21] Gerardine G Botte, Venkat R Subramanian, and Ralph E White. Mathematical modeling of secondary lithium batteries. *Electrochimica Acta*, 45(15):2595–2609, 2000.

[22] Youngki Kim, Jason B Siegel, and Anna G Stefanopoulou. A computationally efficient thermal model of cylindrical battery cells for the estimation of radially distributed temperatures. In *American Control Conference (ACC), 2013*, pages 698–703. IEEE, 2013.

[23] Said Al Hallaj, Hossein Maleki, Jong-Sung Hong, and J Robert Selman. Thermal modeling and design considerations of lithium-ion batteries. *Journal of Power Sources*, 83(1):1–8, 1999.

[24] Kandler Smith and Chao-Yang Wang. Power and thermal characterization of a lithium-ion battery pack for hybrid-electric vehicles. *Journal of power sources*, 160(1):662–673, 2006.

[25] Weifeng Fang, Ou Jung Kwon, and Chao-Yang Wang. Electrochemical–thermal modeling of automotive li-ion batteries and experimental validation using a three-electrode cell. *International journal of energy research*, 34(2):107–115, 2010.

[26] Karthik Somasundaram, Erik Birgersson, and Arun Sadashiv Mujumdar. Thermal–electrochemical model for passive thermal management of a spiral-wound lithium-ion battery. *Journal of Power Sources*, 203:84–96, 2012.

[27] Matteo Corno, Nimitt Bhatt, and Michel Verhaegen. An efficient control oriented modeling approach for lithium ion cells. In *American Control Conference (ACC), 2012*, pages 4733–4738. IEEE, 2012.

[28] Justin K. Rice and Michel Verhaegen. Distributed control: A sequentially semi-separable approach for spatially heterogeneous linear systems. *IEEE Transactions on Automatic Control*, 54(6):1270 – 1283, Jun 2009.

[29] Sohel Anwar, Changfu Zou, and Chris Manzie. Distributed thermal-electrochemical modeling of a lithium-ion battery to study the effect of high charging rates. *IFAC Proceedings Volumes*, 47(3):6258–6263, 2014.

[30] Raffaello D'Andrea and Geir E. Dullerud. Distributed control design for spatially interconnected systems. *IEEE Transactions on Automatic Control*, 48(9):1478 – 1495, sept 2003.

[31] Edwin van Solingen, Jan-Willem van Wingerden, Patricio Torres, Justin Rice, Roeland de Breuker, and Michel Verhaegen. Parameter estimation for spatially interconnected descriptor systems using sequentially semi-separable matrices. In *American Control Conference (ACC), 2013*, pages 1657–1662. IEEE, 2013.

[32] Justin K Rice and Michel Verhaegen. Efficient system identification of heterogeneous distributed systems via a structure exploiting extended kalman filter. *IEEE Transactions on Automatic Control*, 56(7):1713–1718, 2011.